This manuscript has been published in final form at https://linkinghub.elsevier.com/retrieve/pii/S0920586118307648
DOI: 10.1016/j.cattod.2019.02.020

Hydroconversion mechanism of biomass-derived γ-valerolactone

Gyula Novodárszki,[a] Hanna E. Solt,[a] György Lendvay,[a] R. Magdolna Mihályi,[a] Anna Vikár,[a] Ferenc Lónyi,*[a] Jenő Hancsók,[b] and József Valyon[a]

[a] *Institute of Materials and Environmental Chemistry, Research Center for Natural Sciences, Magyar tudósok körútja 2, H-1117 Budapest, Hungary. E-mail: lonyi.ferenc@ttk.mta.hu*
[b] *Department of MOL Hydrocarbon and Coal Processing, University of Pannonia, Egyetem utca 10, H-8200 Veszprém, Hungary*

Abstract

The hydroconversion mechanism of γ-valerolactone (GVL) was studied over a Co/SiO_2 and a Pt/aluminosilicate catalyst. The reaction was carried out at 250 °C, 30 bar, and WHSV= 1 $g_{GVL} \cdot g_{cat.}^{-1} \cdot h^{-1}$. The Co/SiO_2 catalyst had moderate hydrogenation activity and Lewis acidity, whereas the Pt/aluminosilicate catalyst had high hydrogenation activity and Brønsted acidity. Diffuse Reflectance Fourier Transform Spectroscopic (DRIFTS) results suggested that the GVL ring was bounded more strongly to the stronger acid Pt/aluminosilicate that to the weaker acid Co/silica catalyst. The Pt/aluminosilicate catalyst was substantiated to open the GVL ring in a protonation/deprotonation process giving pentenoic acid (PE) intermediate and pentanoic acid (PA) as main final product. Over Co/SiO_2 catalyst 2-methyl-tetrahydrofuran (2-MTHF) and pentanol were the major products of GVL conversion. It was substantiated that latter transformation proceeded in consecutive hydrogenation and dehydration steps via 2-hydroxy-5-methyl-tetrahydrofuran and 1,4-pentanediol (1,4-PD) intermediates. The oxygen atoms of GVL were shown to establish H-bonds with the silanol groups of the Co/SiO_2 catalyst. The ν_{CO} frequency of the adsorbed GVL depends on the adsorption interaction of the GVL and the silica surface. Three distinct ν_{CO} bands were distinguished by DRIFTS. Quantum chemical calculations gave the structures of the three adsorbed GVL species. Operando DRIFTS examination of the catalytic reaction suggested that in the structure that was activated for hydrogenation/hydrogenolysis both the ring and the carbonyl oxygen were bound to silanol groups.

Keywords: gamma-valerolactone (GVL) hydroconversion, GVL bonding to silica, 2-methyltetrahydrofuran, pentanoic acid, DRIFT spectroscopy

1. Introduction

Fossil carbon sources are to be increasingly replaced by renewable carbonaceous materials both in energy and chemical industries, in order to decrease emission of greenhouse gas carbon dioxide and, thereby, to mitigate global warming [1-7]. Gamma-valerolactone (GVL) can be easily derived from lignocellulosic waste, which is an abundant renewable carbon source. GVL is relatively inexpensive and has the functionality and reactivity to be used as platform compound for producing a number of value-added chemical products [2,3,5,8-10]. A plausible direction of lactone conversion is its reduction to diol. Organic

chemists use $LiAlH_4$ as reducing agent in anhydrous non-protic solvent. From GVL, according to organic chemistry textbooks, 1,4-pentanediol (1,4-PD) is obtained with high selectivity via 4-(AlH_3-O)-pentyl aldehyde intermediate.

From the sugar polymer components of lignocellulose, such as, cellulose and hemicellulose, pentoses and hexoses can be obtained by hydrolysis. These monosaccharides can be relatively easily converted to levulinic acid (LA). GVL can be produced by from LA by consecutive catalytic hydrogenation and dehydration reactions. The applied catalysts usually have also activities, such as, isomerization, esterification, and polymerization. For simplicity, the conversion of LA and GVL in consecutive and parallel reactions in the presence of hydrogen is referred here to as hydroconversion. Most of the related research focuses on the catalytic hydroconversion of LA or LA ester [11]. The reaction results in GVL, which is either final product or intermediate of further transformations [3-5,10-13]. The conversion and selectivity depends on the catalyst and reaction conditions. The GVL transformation can run on different routes, which lead through different intermediates to various major products. However, the factors determining the catalytic activity and selectivity of GVL hydroconversion is not really known yet [14-17]. The reaction is usually carried out in liquid phase using batch reactor where the solvent can participate in the transformation or can influence its direction. As a consequence, the result of catalytic GVL hydroconversion is not as predictable as the reaction of GVL with reducing agent $LiAlH_4$.

The present study concerns the gas-phase conversion of GVL over oxide-supported metal catalysts using continuous flow-through tube reactor. The activities of two catalysts are compared: a silica-supported cobalt catalyst, having moderate hydrogenation activity, and an aluminosilicate-supported platinum catalyst, having high hydrogenation activity. Both catalysts have also acid sites. The cobalt catalyst shows Lewis acidity, whereas the Pt catalyst has both Lewis and Brønsted acidity. Both Brønsted and Lewis acid sites can initiate dehydration [3,9,10,18-25]. It has been already shown that Brønsted acid sites alone can initiate cleavage of the (CH_3C)-O bond of GVL giving pentenoic acid (PE) [3,10,18,23]. If the catalyst and reaction conditions allow PE hydrogenation, pentanoic acid (PA) is generated. We found that the aluminosilicate-supported Pt-catalyst generated mainly pentanoic acid (PA or valeric acid). The PA is useful intermediate to PA esters that are used in perfumes and cosmetics and also as food additives because of their fruity flavors [26]. Ethyl valerate is a promising second generation biofuel [18,27,28].

The PE and PA can be further reduced to C_5 alcohols (pentanols). Dehydration of the alcohols and decarboxylation of the acids can give C_5 and C_4 hydrocarbons. Obviously, the

catalytic GVL hydroconversion can give a spectrum of products. Directing the selectivity of the reaction is a real challenge for a catalytic chemist.

The catalytic hydroconversion of GVL over the silica-supported Co-catalyst was found to give 2-methyltetrahydrofuran (2-MTHF) as main product. Hydrogenolysis of the ester bond, O-(C=O), of GVL must give 1,4-PD. However, negligible amount of 1,4-PD intermediate appeared in our product mixture. It seemed rational to believe that 1,4-PD was dehydrated to the cyclic ether 2-MTHF [9,10,20,22]. The 2-MTHF can be blended with conventional hydrocarbon fuels in high percentage [3,4,8,10,18,25].

Both supported cobalt or platinum has hydrogenolysis and hydrogenation activity [3,10,18-24]. However, it remains a question what catalytic properties can direct the reaction to 2-MTHF or to PA formation, and what the intermediates of the transformations are. The formation of 1,4-PD from GVL requires the uptake of two H_2 molecules. Since simultaneous uptake of two H_2 molecules is very unlikely, an additional intermediate must be involved in the formation of 1,4-PD. The PA can come either from PE hydrogenation or from direct hydrogenolysis of the (CH_3C)-O bond. The hydrogenolysis is generally not considered as possible route to PA formation. The catalysts of the present work, showing distinctly different selectivity in GVL hydroconversion, were studied by in situ Diffuse Reflectance Fourier Transform Spectroscopy (DRIFTS) to learn more about the catalytic mechanism.

The product distribution of the reaction, the surface and GVL adsorption properties of the studied catalysts are presented and discussed.

2. Experimental

2.1. Catalyst preparation

Silica support (type CAB-O-SIL EH5 from Cabot Co., specific surface area: 385 $m^2 \cdot g^{-1}$) was impregnated with a 0.4 M aqueous solution of $Co(NO_3)_2 \cdot 6H_2O$. Ten grams of silica was suspended in 40 cm^3 solution then the suspension was dried at 110 °C for 12 hours. Silica supported Co-oxide catalyst was obtained by calcining the sample in air at 500 °C for 3 hours. The supported oxide was reduced in situ in either in catalytic microreactor or infrared spectroscopic reactor cell (vide infra) in flowing H_2 at 450 °C for 1 hour. The cobalt content of the catalyst, determined by atomic absorption spectroscopy, was 8.0 wt%. The reduced catalyst is designated as Co/SiO_2.

Sodium form of aluminum-containing magadiite (Na-[Si,Al]MAG) having an Si/Al ratio of 19.0 was prepared by hydrothermal crystallization of aluminosilicate gel with the

molar composition of 1.0 SiO_2 : 0.026 Al_2O_3 : 0.110 Na_2O : 0.079 Na_2SO_4 : 7.85 H_2O at 125 °C for 120 h [29]. Ground silica and water-glass were used as silica source, whereas $Al_2(SO_4)_3 \cdot 18H_2O$ was applied as aluminum source. The product was filtered and washed with distilled water then dried at 120 °C. The sodium form was ion-exchanged three times with a 1M NH_4Cl solution at room temperature to get the NH_4-form. The thus obtained NH_4-[Si,Al]MAG sample, having a specific surface area of 61 $m^2 \cdot g^{-1}$, was used as aluminosilicate support for the preparation of supported Pt-catalyst [29]. Calculated amount of $Pt(NH_3)_4(OH)_2 \cdot xH_2O$ (34.5 mg) was dissolved in 10 cm^3 of distilled water and this solution was poured over 5 g of support material. The suspension was mixed at room temperature for 3 h then was placed on a water bath, where water was slowly evaporated under continuous stirring. Sample was further dried at 150 °C for 30 min in air then the temperature was raised by 4 °C·min^{-1} up to 480 °C and sample was calcined at this temperature for 4 h. The Pt precursor compound decomposed and the NH_4-[Si,Al]MAG support became deammoniated to get the Pt,H-form of the magadiite (Pt,H-[Si,Al]MAG). The preparation was pre-treated in situ either in catalytic microreactor or infrared spectroscopic reactor cell (vide infra) in flowing H_2 at 450 °C for 1 hour. The support is designated as H-MAG, whereas the reduced catalyst containing 0.5 wt% Pt is referred to as Pt/H-MAG.

2.2. Catalyst characterization

The specific surface areas were determined from the N_2 adsorption by the B-point method. The isotherms were measured at -196 °C using an automatic gas adsorption instrument (SURFER, Thermo Fisher Scientific). Before measuring the adsorption isotherm, sample was evacuated at 350 °C for 12 h.

Acidity of the catalyst samples was characterized using the characteristic infrared (IR) absorption bands of pyridine (Py) adsorbed on Brønsted- and/or Lewis acid sites of the catalyst [30]. IR spectra of the sample were recorded by a Nicolet Impact 400 type Fourier Transform Infrared (FTIR) spectrometer before and after adsorption of Py using the wafer transmission technique. Before the experiments, the wafer of the catalysts was reduced in situ in H_2 flow at 450 °C for 1 h then evacuated in high vacuum (10^{-6} mbar) at 400 °C for 1 h. The activated catalyst sample was contacted with 5.7 mbar Py vapor at 200 °C for 30 min, then was degassed at 200 °C for 30 min and cooled to room temperature. The degassing step was repeated at 300 and 400 °C. Spectrum was recorded at room temperature after each treatment collecting 32 scans at a resolution of 2 cm^{-1}. Absorbance was normalized to wafer thickness

of 5 mg·cm^{-2}. Difference spectra, characteristic of adsorbed Py, were obtained by subtracting the spectrum of the activated sample from the spectra collected after Py adsorption.

Metal particle size in the catalysts was characterized by X-ray diffractometric (XRD) method. XRD patterns were recorded by a Philips PW 1810/3710 powder diffractometer, equipped with a graphite monochromator, applying $CuK_{\alpha 1+\alpha 2}$ radiation ($\lambda_{average}$=1.541862 Å) using a step of 0.02 2Θ degree and a count time of 4.0 s. Catalyst powder was placed in the sample holder and was reduced in situ in the high-temperature Anton-Paar chamber in H_2 flow at 450 °C for 1 h, then cooled to room temperature before measuring the diffraction pattern. The average crystallite size of the metal particles formed was determined by the Scherrer equation evaluating the FWHM values of the diffraction lines applying full profile fitting method.

Distribution of metal particle size on the catalysts was characterized by Transmission Electron Microscopy (TEM). Diluted suspensions of samples in water were prepared and drop-dried on carbon coated copper TEM grids. TEM images were taken by type Morgagni 268D microscope (100 kV, W filament, point-resolution= 0.5 nm).

2.3. Catalytic experiments

The catalytic properties of the catalysts shown in the hydroconversion of GVL were studied using a high-pressure flow-through microreactor. The stainless steel reactor tube (12 mm I.D.) was loaded with 1 g of catalyst grains (0.315 – 0.63 mm size fraction). The catalyst sample was treated in situ at 450 °C and 30 bars in 6 L·h^{-1} flow of H_2 for 1 h, after which the temperature was lowered to 250 °C, the hydrogen feed was set to 3 L·h^{-1} and the reaction was initiated by feeding GVL into the reactor at a rate of 1 g_{GVL}·h^{-1} (WHSV= 1 g_{GVL}·$g_{cat.}^{-1}$ · h^{-1}). In a water-cooled condenser the reactor effluent separated to liquid and gas. The composition of the liquid and the gas were analyzed by a Shimadzu QP2011 GC-MS apparatus equipped with an FFAP-CB fused silica capillary column, having the length of 25 m.

The catalytic experiments were run up to 50 h time-on-stream in order to check the stability of the Co/SiO_2 and Pt/H-MAG catalysts during the reaction. The catalytic activity and selectivity practically remained unchanged throughout the experiments indicating that noticeable catalyst deactivation did not occur under the applied reaction conditions.

2.4. In situ DRIFTS spectroscopic investigations

Species obtained from the transformation of GVL on the catalyst surface were studied by DRIFT spectroscopy. A Nicolet 5PC spectrometer was equipped with a flow-through DRIFTS reactor cell (Spectra-Tech, Inc.). The sample cup of the cell (I.D.: 5 mm, height: 4 mm) was filled with about 20 mg of powdered sample. The design of the cell allows carrier gas or reactant mixture to flow through the catalyst bed in the sample cup. First the catalyst was pre-treated *in situ* in a 30 $cm^3 \cdot min^{-1}$ H_2 flow at 450 °C for 1 h. The GVL reaction was initiated by switching the H_2 or He flow to a gas saturator containing GVL at room temperature. The saturated gas contained 430 ppm GVL. In some experiments the total pressure in the reactor cell was raised from atmospheric pressure up to 20 bar using a back pressure regulator upstream to the cell. Spectra were taken between 35 and 250 °C. The spectrum obtained from the catalyst and the reacting gas, H_2/GVL or He/GVL, was corrected with the spectrum of the catalyst in H_2 or He at the same temperature. The result is a difference spectrum showing the bands of surface species and the absorption bands from the vibration modes of molecules in the gas above the catalyst. It was found however that the contribution of the gas phase spectrum is negligible under the applied conditions and the obtained difference spectrum practically reflects surface species formed (positive bands) or consumed (negative bands) in the GVL adsorption/reaction processes.

2.5. Theoretical methods

The molecular geometry of GVL and of GVL attached to $Si(OH)_4$ or to $Si_4O_4(OH)_{12}$ representing the silica surface has been optimized using the M05-2X density functional [30] and with Moller-Plessett perturbation theory and the correlation-consistent basis sets cc-pVDZ and cc-pVTZ [32]. The applied levels are: M05-2X/cc-pVDZ, M05-2X/cc-pVTZ, MP2/cc-pVDZ and MP2/cc-pVTZ. Vibrational spectra have been calculated at each of these levels. All calculations were performed with the Gaussian 03 suite of programs [33].

3. Results and discussion

3.1. Catalytic hydroconversion of GVL

Hydroconversion of GVL generally leads to the formation of 2-MTHF and/or PA as main reaction products [3,9,10,18,22,23,34]. Preliminary catalytic experiments carried out in our laboratory on different catalyst systems resulted in a wide variety of selectivities (see in supporting information, Table S1). Among these catalyst systems, Co/SiO_2 and Pt/H-MAG

catalyst showed distinctively high selectivity either towards 2-MTHF or PA product, therefore we focused on these catalysts in the present study.

Recent studies suggested 1,4-PD as intermediate of 2-MTHF formation (Scheme 1) [3,9,10,18,22,23]. Using Pd/C catalyst, Al-Shaal et al. [20] showed that byproducts 1-pentanol and 2-pentanol are formed in the dehydration/hydrogenation reaction of 1,4-PD. Hydrogenation of 2-MTHF can also give 2-pentanol, which can explain why 2-pentanol selectivity is higher than that of 1-pentanol. We obtained similar results using Co/SiO_2 catalyst (Table 1). At medium conversion level (41.2 mol% conversion at 200 °C) 2-MTHF was formed with a high selectivity (69.5 mol%), whereas pentanols accounted for nearly 20 mol% of the product mixture. Minor products, such as pentane, 2-pentanone, 2-butanone and 1-butanol can also be considered as byproducts originating from 1,4-PD and 2-MTHF via dehydration, hydrogenation, and decarbonylation reactions [20]. The latter four byproducts amounted to less than 5 mol % of all the products at 200 °C. At nearly total GVL conversion (99 mol% conversion at 250 °C) formation of byproducts significantly increased at the expense of 2-MTHF, however, its selectivity still remained relatively high (52.9 mol%). Because all byproducts were obtained from 1,4-PD or 2-MTHF, the first step of GVL transformation over the Co/SiO_2 catalyst cannot be anything else than cleavage of the ester bond, O-(C=O) (Scheme 1, position A).

Earlier studies reported about high PA selectivity (>80-90%) of GVL hydroconversion over bifunctional Pt/H-ZSM-5/SiO_2 and Pd/Nb_2O_5 catalysts [18,34]. Depending on the metal content and the acidity of the catalyst, pentyl valerate [18] or C_4-C_5 alkanes [34] were formed as minor byproducts. These byproducts were clearly related to the hydrogenation or decarboxylation of PA.

Over the Pt/H-MAG catalyst of the present study GVL was transformed to PA with high selectivity (>90%) at medium conversion level (43.5 mol% conversion at 250 °C), whereas its selectivity only slightly decreased to 79.4 mol% at high conversion level (90.2 mol% conversion at 300 °C). The main byproduct was pentyl valerate (Table 1). In agreement with earlier studies, the product distribution clearly shows that the (CH_3C)-O bond of the GVL molecule breaks up over the Pt/H-MAG catalyst as the first step of the hydroconversion reaction (Scheme 1, position B).

3.2. Acid sites and metal particles in the catalysts

Different activities of GVL hydroconversion catalysts were shown to come from their different acidities [18,23,34]. IR spectra of adsorbed Py gives information about the acid sites of catalysts. Pyridine binds coordinately to Lewis acid sites, whereas Brønsted acids protonate pyridine and the pyridinium ions (PyH^+) bind to the solid, i.e., to the conjugated base of the acid. Lewis- and Brønsted-bound Py give characteristic infrared absorption bands at around 1450 cm^{-1} and 1550 cm^{-1}, respectively [24,30,35]. The spectra of Py, adsorbed on Co/SiO_2 and Pt/H-MAG catalysts showed the presence of acidic sorption sites (Fig. 1A). In line with earlier studies [24,30,35,36], no IR band of adsorbed Py could be detected on the applied silica support above about 150 °C (not shown), since the weak acid silica cannot retain Py at this temperature. Lewis acid adsorption sites only could be detected over the Co/SiO_2 sample (Fig. 1A, spectra *a-c*), whereas both Lewis and Brønsted acid adsorption sites were present in the Pt/H-MAG catalyst (Fig. 1A, spectra *d-f*). The corresponding characteristic Py bands, labeled by [L] and [B] in Fig. 1A, remained well discernible even after evacuation treatment of the sample at 400 °C, suggesting that the samples contain adsorption sites of considerable acid strength.

The XRD pattern measured on Co/SiO_2 sample reduced at 450 °C (Fig. 1B, *a*) indicates the presence of CoO phase in the catalyst sample (vide infra), suggesting that reduction of the oxide was not complete. Reflections of Co^0 particles could be observed at 2Θ degrees of 44.3 and 51.6 ([111] and [200] reflections), whereas low intensity reflections of CoO at 2Θ degrees of 36.5 and 42.4 ([111] and [200] reflections) are clearly visible (Fig 1B, *a*). Using the Scherrer equation the average size of the cobalt particles was estimated to be 20.5 nm. H_2-TPR measurement on the same catalyst sample showed that about 90% of cobalt could be reduced up to 450 °C [37]. Sun et al. [38] reported about the same reduction level (~90%) for a similar silica-supported cobalt oxide catalyst. These authors attributed the hard-to-reduce fraction to coordinately unsaturated cobalt cations strongly attached to the silica surface via oxygen bridges [36,39,40].

The layered structure of the magadiite support gave rise to the appearance of the [001], [002], and [003] XRD lines at 2Θ degrees of 6.0, 11.4, and 17.1, respectively (not shown here) [29,41]. Reflections in the 23-30 range of 2Θ degrees reflect the ordered structure of the individual magadiite sheets (Fig. 1B, *b*). Pt^0 particles were identified by the characteristic [111] and [200] reflections at 2Θ degrees of 39.8 and 46.3. The average particle size, determined by the Scherrer equation, was 15 nm.

In agreement with the XRD results TEM images in Fig. 2 show that Co particles of about 20 nm diameter, and Pt particles of about 15 nm diameter dominate in Co/SiO_2 and Pt/H-MAG catalyst, respectively. The particle size distribution of Pt in Pt/H-MAG catalysts seems to be relatively homogeneous, whereas Co particles smaller than 10 nm and larger than about 30-40 nm also can be observed in the Co/SiO_2 catalyst.

Generation of strong Brønsted and Lewis acid sites in aluminum-containing magadiite is related to the substitution of Q4 Si atoms (Si atoms, surrounded by four –OSi groups) and Q3 Si atoms (Si atoms, having three –OSi neighbors) by aluminum atoms in the magadiite structure, respectively [29,42,43]. As it was shown in a former study from our laboratory [29], aluminum atoms in Q4 sites generated strong Brønsted acid sites ([Si-O(H)-Al] bridged hydroxyls), whereas three-coordinated Al atoms in Q3 sites were found to be strong Lewis acids. The IR spectra of adsorbed Py showed the presence of both types of acid in the Pt/H-MAG catalyst (Fig. 1A, spectra *d-f*).

3.3. Adsorption of GVL

3.3.1. Adsorption sites

Similar DRIFT spectra were obtained from the adsorption of GVL/H_2 mixture on Co/SiO_2 catalyst and on the silica support at 35 °C (Fig. 3, cf. spectra *a* and *b*), indicating that the most abundant adsorption sites are the same on these materials. Note that transformation of GVL is unlikely at the temperature of the measurement. The positive bands in the spectra are assigned to adsorbed GVL, whereas the negative bands are associated with surface species consumed by the interaction with the GVL. The negative ν_{OH} band at 3745 cm^{-1} indicates the involvement of terminal silanol groups in the interaction with GVL. Absorption bands also appeared in the range of ν_{CH}, ν_{CO}, and δ_{CH} vibrations. The erosion of ν_{OH} band at 3745 cm^{-1} is also accompanied with the development of an intensive and broad band at ~3350 cm^{-1}. This shifted OH band usually appears when H-bond is formed between surface OH-groups and non-protonating weak base molecules [44,45]. The shift of the ν_{OH} band from its original position depends on the acidity of the surface OH-groups and the proton affinity of the adsorbing molecule [44]. Binding GVL the ν_{OH} band of the silanol groups suffered a red shift of about 400 cm^{-1}. Similar silanols are also present in Pt/H-MAG as indicated by about the same shift of the corresponding ν_{OH} band (Fig. 3, spectrum *c*). The Pt/H-MAG sample, however also contains relatively strong Brønsted acid bridged OH groups. The negative band at 3610 cm^{-1} indicates that these OH groups also adsorb GVL. This adsorption interaction

results in significantly larger shift of hydroxyl band than that observed for the silanol groups. Instead of a single broad feature, component bands (so-called ABC triad) appear as a result of Fermi resonance between the downward shifted ν_{OH} band of the O-H···GVL adsorption complex and the upward shifted 2γ and 2δ overtone vibrations of the same OH-groups [44,45]. Two of these component bands at about 3100 and 2400 cm^{-1} are clearly discernible on the spectrum obtained from GVL adsorption on Pt/H-MAG catalyst (Fig. 3, spectrum *c*) suggesting the formation of strong hydrogen bonds between GVL and Brønsted acid hydroxyl groups. We note here, that the spectrum obtained from the adsorption of GVL on the H-MAG support at 35 °C was practically the same than that measured on the Pt/H-MAG catalyst. Therefore, the corresponding spectrum was not shown in Fig. 3 for the sake of simplicity.

These results suggest that GVL is mainly adsorbed on weak acid silanol groups of the silica support of Co/SiO_2 catalyst, whereas both silanol and strong Brønsted acid hydroxyl groups are involved in the adsorption interaction of GVL and the catalyst Pt/H-MAG.

3.3.2. Adsorption interactions of GVL

Tetrahydrofuran (THF) gives a relatively strong vibration band at around 915 cm^{-1} [46,47], which always appear in the spectra of THF derivatives in the 900 – 950 cm^{-1} range [48,49]. It has been shown that this band is predominantly due to C-C-C-C vibrations with only a very weak contribution from C-H rocking motion, and therefore it can be thought of as a ring-breathing mode [50,51]. There is a strong absorption band at 943 cm^{-1} in the spectrum obtained from adsorption of GVL over the Co/SiO_2 catalyst. Based on the above mentioned former studies, we assign this band to the breathing vibration of the THF ring of GVL. Interestingly, this band appeared with a significantly lower intensity in the corresponding experiment using catalyst Pt/H-MAG (Fig. 3, cf. spectra *a* and *c*). Similar drop of the relative intensity of the ring-breathing mode upon adsorption has been often observed for different molecules with or without heteroatom in the ring, such as benzene, toluene, thiophene, and morpholine [52-55]. The intensity loss was attributed to the strong interaction of the ring electrons with surface hydroxyls [52-54], or to strong host-guest interaction within the constrained space of the zeolitic cages [55]. The different intensities of the ring-breathing vibration suggest that on Co/SiO_2 catalyst GVL seems to be adsorbed via its ring O-atom and/or the carbonyl group (vide infra), whereas the whole ring must be in strong interaction with the surface of the Pt/H-MAG catalyst, hindering ring vibration of the GVL ring. The

strong interaction of the GVL ring can be clearly attributed to Brønsted acid sites present in Pt/H-MAG.

3.3.3. Bending vibrations.

The spectral region of ν_{CO} and δ_{CH} vibrations is shown in Fig. 4. The δ_{CH} bands of adsorbed GVL (Fig. 4, spectra *a-c*) are similar to those of liquid phase GVL (Fig. 4, spectrum *d*). However, due to adsorption interactions the bands are somewhat shifted to higher wavenumbers. Group frequency assignments from the IR spectroscopy literature helped us to assign each bands to a specific GVL group [47,56-58]. The bands at 1450 cm^{-1} and 1390 cm^{-1} stem from $\delta_{as}[CH_3]$ and $\delta_s[CH_3]$ vibrations, respectively (Fig. 4). The scissoring vibration of methylene groups, $\beta_s[CH_2]$, usually gives an intense band at around 1465 cm^{-1}, overlapping with the high frequency side of $\delta_{as}[CH_3]$ band. However, the $\beta_s[CH_2]$ frequency is very sensitive to the presence of any electronegative group in the immediate vicinity of the methylene group. For instance, if the methylene group is adjacent to a carbonyl group, like in the GVL molecule, its scissoring vibration appears red shifted by about 40 cm^{-1}. Accordingly, we assign the bands at 1462 cm^{-1} and 1423 cm^{-1} to scissoring vibrations of methylene groups neighboring each other and either a methine, $\beta_s[CH_2(C\text{-}H)]$, or a carbonyl group, $\beta_s[CH_2(C{=}O)]$ (Fig. 4). The characteristic $\delta[CH]$ frequency of methine groups is usually around 1340 cm^{-1}. The $\delta[CH]$ band is usually weak relative to the $\delta[CH_3]$ and $\beta_s[CH_2]$ bands. It is to be noted, however, that the $\delta[CH]$ band gains intensity when it is next to a heteroatom, such as oxygen [57,58]. We assign the band at ~1355 cm^{-1} to the bending vibration of the methine group connected to oxygen atom in the GVL ring (Fig. 4, band $\delta[CH(O)]$).

Monitoring the intensity of characteristic infrared absorption bands, the transformation of GVL can be followed on the catalyst surface.

3.3.4. Carbonyl stretching vibrations.

In diluted CCl_4 solution the ν_{CO} vibration of the GVL carbonyl group gave a single band at 1782 cm^{-1} (Fig. 4, spectrum *d*). In contrast, the GVL adsorbed on Co/SiO_2 and Pt/H-MAG catalysts, or on the SiO_2 support of the cobalt catalyst gave overlapping ν_{CO} bands at 1760, 1740, and ~1710 cm^{-1} wavenumbers (Fig. 4). These results suggest that the GVL molecule interacts with the same most abundant adsorption sites in these solids, namely with silanol groups. The GVL must establish three dominating specific interactions with the silica surface, which are differently affecting the ν_{CO} frequency. Earlier studies assigned similar

bands to GVL physically adsorbed, and to GVL in weak chemical interactions with the silica surfaces [24,35]. Scotti et al. [35] detected also a relatively small band at around 1680 cm^{-1} on a Cu/SiO_2 catalyst and ascribed the band to GVL strongly chemisorbed via its carbonyl group on Lewis sites generated by the copper species. A small band near to 1680 cm^{-1} is also discernible on the spectra of GVL adsorbed on the catalysts of the present study (Fig. 4, spectra *a* and *c*). No similar band was obtained when GVL adsorbed on the silica support (Fig. 4, spectrum *b*). Accordingly, this band is attributed to the ν_{CO} band of GVL interacting with Lewis acid sites of the catalysts. Lewis acidity of the Co/SiO_2 and Pt/H-MAG catalysts was evidenced by detecting Lewis-bound Py (vide supra, Fig. 1). It was shown above that the unreduced fraction of Co-oxide generates relatively strong Lewis acid sites on the silica support in the Co/SiO_2 catalyst, whereas the aluminum containing H-MAG support inherently contains strong Lewis acid sites (see in section 3.2.). Nevertheless, the 1680-cm^{-1} band is weak relative to the other ν_{CO} bands, suggesting that the Lewis-bound GVL represents only a minor fraction of the GVL adsorbed on the surface of the Co/SiO_2 or Pt/H-MAG catalyst. In conclusion, the analysis of the range of the carbonyl stretching vibrations suggests that the main adsorption sites for GVL must be the abundantly available silanol groups in Co/SiO_2, whereas both silanol and Brønsted acid hydroxyl groups interact with GVL in Pt/H-MAG catalyst. We note here, that the spectrum obtained on this latter catalyst was practically the same than that on the H-MAG support (not shown), suggesting that the presence of small amount of Pt metal particles did not result in the formation of new adsorption sites in the Pt/H-MAG catalyst.

3.3.5. Electronic structure calculations.

The carbonyl oxygen has generally negative polarity that promotes hydrogen bonding that induces red shift of the ν_{CO} frequency. The strength of interaction between the GVL carbonyl group and silanol groups of the catalyst determines the extent of red shift. Different adsorption strengths assume different adsorption geometries and vibrational frequencies.

Electronic structure calculations were carried out by simulating the silica surface by an $Si(OH)_4$ or by an $SiO_4(OH)_{12}$ model. In both cases the geometries of GVL and the silica model was optimized beforehand; then the two units were placed close to each other in various orientations and the geometry of the complete structure was optimized. Numerous conformers were found with both silica models. All of these were found to represent three basic types of bonding between GVL and the surface (Fig. 5).

When a single H-bond is formed, the H-atom is connected to the oxygen of the carbonyl group of GVL (Fig. 5, S1). This kind of structure has been observed with both the $Si(OH)_4$ and the $SiO_4(OH)_{12}$ model.

Two different arrangements were observed when two H-bonds are formed. In one of these structures (Fig. 5, S2), one of the hydrogen bonds involves the carbonyl oxygen, and the other is formed between the O-atom of the lactone ring. The two OH-groups participating in the interaction are attached to the same Si atom. The other kind of adsorbed structure with two H-bonds (Fig. 5, S3) can be observed only when at least two Si atoms offer OH-groups for hydrogen bond formation. In Fig. 5, S3 the carbonyl oxygen is connected simultaneously to two H-atoms of OH-groups on two next-neighbor Si atoms.

One can argue that our models of silica surface are oversimplified. However, if one considers the size of the GVL molecule, it is easy to see that even if more extensive surface was provided for adsorption, the molecule could not interact with more Si(OH) units than in our models. Further support is provided by the following observations: *(i)* structures S1 and S2 (Fig. 5) with a single and two separate hydrogen bonds, respectively, have been found with both silica models, with essentially the same bond lengths and angles; *(ii)* the properties of several conformers were found not to be sensitive to freezing those coordinates of the surface model that were not involved in the hydrogen bonds; *(iii)* the carbonyl vibrational frequency was also the same (within the accuracy limits of the frequency calculation at the given level of calculation) of the analogous structures, even in geometries with frozen silica bonds. Since the interaction of the functional groups with the surface is local, these observations support the goodness of our model.

Structures S1-S3 are characterized by bond lengths shown in Table 2. In the conformers of each adsorbed structure, the bond length of the C=O bond varies by less than about 0.02 Å, that of the C=O···H bond by less than 0.2 Å.

When the oxygen of the carbonyl group as well as the H-atom of an OH-group get involved in a hydrogen bond, the strength of both bonds is somewhat reduced which is reflected by their elongation (for reference, Table 2 also shows the lengths of O-H bonds not involved in hydrogen bonds). The magnitude of the increase of the bond length is closely related to the strength of the hydrogen bond. This is supported by the observation that the vibrational frequencies follow the same tendencies. Shown in Table 3 are the calculated vibrational frequencies of the carbonyl group.

One can see that the frequencies follow the trend set by the bond lengths. The frequency shift is the smallest in structure S2, in which the hydrogen bond at the carbonyl O-

atom cannot fully develop because the other hydrogen bond formed by the ring oxygen atom does not allow the formation of the favorable collinear arrangement. When the C=O group is involved in a complete hydrogen bond, the frequency shift is significantly larger (structure S1). Even larger shift can be seen when the C=O group forms simultaneously two hydrogen bonds (structure S3). In this case the C=O bond length elongation is also the largest. The C=O···H hydrogen bond length is the shortest in S1, because the strain is minimum in this structure. In S3 both hydrogen bonds are longer than in S1, because the distance between the Si atoms is large. In principle the O-atom could get closer to both H-atoms, but then the angle between the two hydrogen bonds would be very large. The O-H bond lengths longer than the optimum for a single H-bond balance the large H–O–H angle (about 125°). The twin hydrogen bonds in S3 exert a larger effect on the C=O bond than the close to perfect H-bond in S1. This is reflected both by the length of the carbonyl bond and by the frequency of the C=O stretching vibration. The tendencies listed above have been observed with all tested electronic structure methods. One can see, however, that neither the DFT nor the ab initio calculations reproduce precisely the measured frequency of the "free" GVL in solution. In order to facilitate the comparison with the experiments, we use the procedure put forth by Pulay [59]: the ratio of the experimental to calculated frequency of a bond in a reference compound (in our case, free GVL) is calculated, and the same factor is used to scale the frequencies in other cases. (Note that this procedure may require different scale factors in different domains of the vibrational spectrum.) For the identification of the structures behind the experimental spectral features, we chose the MP2 frequencies, because we consider these the most reliable (the scale factor is the closest to unity), and selected those calculated with the cc-pVDZ basis set because the frequency calculation of structure S3 with twin hydrogen-bonds is available at this level but is out of reach with the cc-pVTZ basis (Table 3).

Fig. 6 shows the split carbonyl band of the experimental spectrum enlarged, together with the calculated positions (after scaling) of the C=O vibration for free GVL and for structures S1- S3. The height of the calculated bars is proportional to the calculated line intensity. (This is not expected to be directly comparable with the experimental peak heights because the relative surface concentrations of GVL in structures S1-S3 is different, which overwrites the calculated peak intensity ratios, which are concentration-independent.) One can see an almost perfect match between the location of the experimental peak maxima and the scaled MP2/cc-pVDZ frequencies. Based on this, our assignment of the measured peaks is as follows: the component peak at around 1760 cm^{-1} corresponds to structure S2, with two separate H-bonds between GVL and the surface. The scaled shift of this peak with respect to

free GVL is the same in both theory and experiment. Similar good agreement can be seen for the lower-frequency peak of the split C=O band, if one assigns the peak to structure S1. Finally, the shoulder shifted by 70 cm^{-1} toward low frequencies can be assigned to structure S3.

3.4. Surface species obtained from GVL adsorption and reaction

3.4.1. Intermediate of GVL hydrogenation over silica-supported Co catalyst.

Bending vibration spectra of surface species obtained from adsorption and hydroconversion of GVL over catalyst Co/SiO_2 were recorded by DRIFT spectroscopy in the 35-225 ℃ temperature range (Fig. 7A). In contact with GVL/He flow at atmospheric pressure the same surface species were found at all the selected temperatures up to 225 ℃. Only the adsorption coverage of the catalyst was smaller at higher temperatures. In contrast, in GVL/H_2 flow the $\beta_s[CH_2(C=O)]$ band at 1422 cm^{-1} became relatively much weaker than the rest of the bands when measurement temperature was set to a higher value. This finding suggests that in hydrogen not only a new GVL adsorption equilibrium was established but some GVL transformation took also place on the catalyst. Similar changes could be observed at 20 bar although the band intensities dropped more significantly on temperature increase than at atmospheric pressure (Fig. 7A, dotted line). These observations clearly show that the reaction of GVL on Co/SiO_2 proceeds in presence of hydrogen only.

It follows from the observed product distribution (Table 1) that the hydroconversion of GVL on Co/SiO_2 results in the elimination of the carbonyl group. If reduction of the C=O bond occurs then the intensity of the $\beta_s[CH_2(C=O)]$ band at 1422 cm^{-1} is expected to decrease more than that of the $\beta_s[CH_2(C-H)]$ band at 1462 cm^{-1}. The unchanged intensity ratio of these bands as function of temperature in He confirms that only the surface coverage was changing (Fig. 7B). In contrast, the drastic drop of the intensity ratio of these bands in H_2 (Fig. 7B) clearly evidences a hydrogenation reaction that eliminates the carbonyl group. Simultaneously the neighbor effect on the vibration of the CH_2 group was also eliminated, weakening of the 1422 cm^{-1} band. It should be noted that the ring-breathing vibration at 943 cm^{-1} remained unchanged (not shown), suggesting that the reaction did not affect the 5-membered ring of the GVL molecule. Therefore, it is rational to think that the surface species formed in the hydrogenation reaction is the 2-hydoxy-5-methyl-THF intermediate. This intermediate is the cyclic hemiacetal of 4-hydroxy pentanal, i.e., the lactol of the 4-hydroxy aldehyde. The aldehyde/lactol equilibrium must be shifted in the direction of lactol (Scheme 2A).

Without direct evidence, based on the product distribution only, the same lactol was suggested by Geilen et al. [25] to be the intermediate of homogeneous catalytic hydroconversion of GVL. Latter intermediate is hydrogenated to give 1,4-pentanediol. Similar, although undetected lactol intermediate was assumed by Hamminga et al. [60] in the hydrogenation of γ-butyrolactone or δ-valerolactone over Cu-ZnO catalysts to the corresponding diols. It was proposed that one H_2 molecule was picked up in the first step by the C=O bond, whereas the hydrogenolysis of the C-O bond in the lactol ring consumes a second molecule of H_2 to form the diol. The in situ spectroscopic results presented here are in agreement with above notions; moreover, direct evidence is provided for the hydrogenation of GVL to 2-hydroxy-5-methyl-THF. Note that these results are also in agreement with the expectation that hydrogenation of C=O group is energetically favored to the hydrogenolysis of the C-O or C-C bonds in the THF ring [61,62].

3.4.2. H-[Si,Al]Magadiite supported Pt catalyst selective for pentanoic acid formation.

DRIFT spectra of Pt/H-MAG catalyst in contact with a flow of GVL/He or GVL/H_2 are shown in Fig. 8A. All the bands, assigned to C-H bending vibrations of adsorbed GVL, decreased in intensity when sample temperature was increased. Regardless of the applied carrier gas (He or H_2), the intensity of the band at 1355 cm^{-1}, assigned to the δ[CH(O)] vibration of the methine group in the lactone ring, decreased significantly faster than the rest of the bands. The relative intensity of the δ [CH(O)] and $\delta_s[CH_3]$ bands at 1355 and 1390 cm^{-1}, respectively, was plotted as function of temperature to show this trend (Fig. 8B). Thus, the quick disappearance of δ[CH(O)] substantiated that the GVL methine group lost its O-atom neighbor in a ring opening process. The opening of the ring did not require hydrogen. However, in hydrogen pentanoic acid was the main product suggesting that ring opening provided most probably pentenoic acid intermediate [23,63] that was then saturated over the catalyst. Thus, formation of pentanoic acid via direct hydrogenolysis can be excluded. These results are in accordance with earlier suggestions [18,34]. It was proposed that formation of pentenoic acid from GVL requires Brønsted acid sites and proceeds via cracking of a protonated intermediate [23,63]. We could not provide direct evidence for the formation of protonated GVL or pentenoic acid intermediate; however, strong adsorption interaction of Brønsted acid sites and GVL, in which the whole lactone ring is involved in the interaction with the surface of magadiite catalyst, was substantiated.

3.4.3. Effect of adsorption geometry on the reactivity of GVL.

It was discussed above that the ν_{CO} band of silica bound GVL comprises of three component bands (Fig. 4). The bands were assigned to complexes having structures S1-S3 (Fig. 5). Obviously, the adsorption should take place in the vicinity of metallic sites for reduction with hydrogen. However, in which of the structure is the carbonyl most activated for reduction by H_2? Because hydroconversion over Pt/H-MAG catalyst gave product molecules that retain the carbonyl group, the question above makes sense only in relation with the hydroconversion over the Co/SiO_2 catalyst.

Difference DRIFT spectra, obtained at elevated reaction temperatures on Co/SiO_2 in contact with GVL/He mixture are shown in the range of ν_{CO} stretching vibration in Fig. 9A. The component bands were determined by resolving the overlapping bands using a peak resolution computer program. Fig. 9B shows that the normalized intensities of the component bands changed together because in He only the adsorption coverage changed with the change of temperature (Fig. 7). Due to hydrogenation reaction, more pronounced drop of the ν_{CO} intensity was induced by the same temperature rise in H_2 than in He (cf. Fig 9 and Fig. 10). Interestingly, the intensity of the band at 1760 cm^{-1} showed a more marked intensity drop than the component bands at 1740 and 1710 cm^{-1} (Fig. 10B). The component band at 1760 cm^{-1} was attributed to the GVL adsorption complex S2 (Fig. 5) in which both the O-atom of the lactone ring and the carbonyl oxygen form hydrogen bond with a silanol group. These results do not exclude that the reaction also proceeds with adsorption complex S1 and S3; however, in adsorption complex S2, hydrogenation of the carbonyl group and hydrogenolysis of the C-O bond in the lactone ring may proceed more effectively by activated hydrogen provided by metallic sites than in adsorption complexes S1 and S3.

3.5. Mechanistic considerations

In situ DRIFT spectroscopic investigation revealed that the most probable surface species, formed in the first reaction step of GVL hydroconversion over Co/SiO_2 is 2-hydroxy-5-methyl-THF (Scheme 2A). It was substantiated that this species was obtained by direct hydrogenation of the carbonyl group. The main product of the reaction is 2-MTHF that can be formed through cyclodehydration of the 1,4-PD intermediate [9,10,20,22]. Diol formation requires hydrogenolysis of a C-O bond in the ring of 2-hydroxy-5-methyl-THF. Cleavage of a C-O bond would result either in unstable geminal diol (Scheme 2A, position A) or 1,4-PD (Scheme 2A, position B). Obviously, the formation of 1,4-PD is favored. Note that at lower

conversion level small amount of 1,4-PD intermediate could be detected in the product mixture (Table 1). Cyclodehydration is known to be catalyzed by both Brønsted and Lewis acids [64,65]. In Section 3.2 we have demonstrated that our Co/SiO_2 catalyst contains strong Lewis acid sites (Fig. 1A). In agreement with former studies, these are the most probable active sites of 1,4-PD cyclodehydration to 2-MTHF (Scheme 2A). The catalyst is bifunctional in the sense that this final step of the consecutive hydroconversion process is catalyzed by Lewis acid sites, whereas the preceding hydrogenation and hydrogenolysis steps are initiated by metallic function.

Beside the above outlined reaction route, the carbonyl reduction of GVL to 2-MTHF in a single process step was also proposed [19]. However, the simultaneous uptake of two H_2 molecules is very unlikely. First 2-hydroxyl-5-methyl-THF must be formed. The reaction with a second H_2 is the hydrogenolysis of a C-O bond resulting either dehydroxylation or in ring opening to get 1,4-PD. The hydrogenolysis of the C-O bond in the ring is, however, more likely than that at the hydroxyl side group from energetic reasons [61,62]. The reaction involving 1,4-PD intermediate seems to prevail.

Conversion of GVL to pentanoic acid on Pt/H-MAG catalyst also proceeds via a bifunctional mechanism. In situ spectroscopic results shown here confirmed that the reaction is initiated by breaking the C-O bond on the methyl side of the lactone ring (Scheme 2B). Earlier studies demonstrated that cracking proceeds on Brønsted acid sites [18,23,63], which were shown to be available also in our catalyst (Fig. 1). Bond et al. [23,63] suggested that on solid acids the ring-opening proceeds through a protonated intermediate, which desorbs as pentenoic acid upon backward proton transfer to the catalyst surface. In the present study, protonated intermediate or olefinic acid intermediate product could not be detected; however, strong hydrogen bonding between GVL and Brønsted acid sites of the H-MAG support was substantiated. These results suggest that full proton transfer to GVL does not occur and the ring-opening probably proceeds through a hydrogen-bonded complex. Indeed, it was shown by Haw et al. [66] that full proton transfer does not take place with bases having a proton affinity lower than about 875 $kJ \cdot mol^{-1}$ even in strong solid acid zeolites. The proton affinity of γ-butyrolactone [67] is only 840.0 $kJ \cdot mol^{-1}$ and GVL should have about the same basicity. Therefore, it is unlikely that GVL is protonated on Pt/H-MAG, which contains weaker acid sites than zeolites.

The above results indicate that formation of pentanoic acid by direct hydrogenolysis of the C-O bond in lactone ring does not occur in the presence of metallic function (Pt) and hydrogen. The ring-opening of GVL on Brønsted acid sites is followed by the hydrogenation

of the unsaturated intermediate pentenoic acid on the platinum (Scheme 2B). It is worth noting that Lange at al. [18] have emphasized that acidic and hydrogenation functions have to be well balanced in the catalyst in order get pentanoic acid with high selectivity. The reaction is less demanding for acid strength, but insufficient hydrogenation function (e.g., too low metal loading) favors the production of pentenoic acid, whereas too high hydrogenation activity (e.g., too high metal loading) favors the formation of 2-MTHF and its over-hydrogenated products (pentanal/pentanol, and/or pentane/butane). Combining this notion with the high pentanoic acid selectivity we observed when using Pt/H-MAG catalyst (>90%, Table 1), we can conclude that acid and hydrogenation functions must be well balanced in our catalyst.

4. Conclusions

Catalyst structure - activity relationship was evaluated in the hydroconversion of GVL. Catalysts having no Brønsted acidity but moderate hydrogenation activity, such as the Co/SiO_2 catalyst, direct the consecutive reaction on the route, starting with the hydrogenation of the C=O bond. Quantum chemical calculations and DRIFT spectroscopic results suggested that the GVL, H-bonded through its two oxygen atoms to two hydroxyl groups of a single surface silicon atom in the vicinity of metallic Co site are the most probable activated species of the reaction. The reaction, resulting in 2-methyltetrahydrofuran was shown to proceed through 2-hydroxy-5-methyl-tetrahydrofurane and 1,4- pentanediol intermediates. Formation of the intermediates assumes both hydrogenation and hydrogenolysis reactions. The reactions are accomplished in an adsorbed state. On Lewis acid sites the diol is rapidly dehydrocyclized to furan not allowing the intermediates to appear in the product mixture in significant amount. Formation of 2-methyltetrahydrofuran via direct hydrodeoxygenation of the GVL carbonyl group seems to be unlikely.

On H-MAG-supported Pt catalyst, containing Brønsted acid sites the lactone ring interacts via strong hydrogen bonding with the catalyst surface, indicated by the significant intensity loss of the ring-breathing vibration of the 5-membered ring from the DRIFT spectrum of the adsorbed GVL. The acid catalyst steered the reaction on another route than the catalyst Co/SiO_2. The reaction was initiated by cracking of the C-O bond on the methyl side of the GVL molecule. Pentenoic acid was substantiated as intermediate, which must have been quickly hydrogenated to pentanoic acid on the platinum sites.

The results show that the hydroconversion of GVL proceeds via bifunctional pathways both over Co/SiO_2 and Pt/H-MAG catalyst. In particular, under the applied reaction conditions it is the combined hydrogenation and Lewis acid functions of Co/SiO_2 what directs the reaction toward 2-MTHF formation, whereas hydrogenation and Brønsted acidic functions of Pt/H-MAG are responsible for pentanoic acid as main product.

Acknowledgements

The financial support of the National Research, Development and Innovation (NRDI) Office (TÉT_15_IN_1_2016_0034, entitled ‘‘Biochemicals and biofuels from lignocellulosic biomass by green catalytic processes’’, and TÉT_16-1-2016-0054, entitled “Development of bio-based catalytic processes for lignocellulosic biomass valorization”) is greatly acknowledged. The authors also acknowledge the financial support of the project of the Economic Development and Innovation Operative Program of Hungary, GINOP-2.3.2-15-2016-00053: Development of liquid fuels having high hydrogen content in the molecule (contribution to sustainable mobility). The Project is supported by the European Union. The research within project No. VEKOP-2.3.2-16-2017-00013 by Gy.L., A.V. and F.L. was supported by the European Union and the State of Hungary, co-financed by the European Regional Development Fund. One of the authors (H. E. Solt) also kindly acknowledges the financial support provided by the Hungarian Scientific Research Fund in the framework of the postdoctoral fellowship program (OTKA_PD_115898). Thanks are due to Gy. Sáfrán for his technical assistance in obtaining TEM images.

References

[1] D.J. Hayes, Catal. Today 145 (2009) 138-151.
[2] J.C. Serrano-Ruiz, A. Pineda, A.M. Balu, R. Luque, J.M. Campelo, A.A. Romero, J.M. Ramos-Fernández, Catal. Today 195 (2012) 162-168.
[3] X. Tang, X. Zeng, Z. Li, L. Hu, Y. Sun, S. Liu, T. Lei, L. Lin, Renewable Sustainable Energy Rev. 40 (2014) 608-620.
[4] K. Yan, Y. Yang, J. Chai, Y. Lu, Appl. Catal. B 179 (2015) 292-304.
[5] K. Yan, C. Jarvis, J. Gu, Y. Yan, Renewable Sustainable Energy Rev. 51 (2015) 986-997.
[6] R.A. Sheldon, J. Mol. Catal. A: Chem. 422 (2016) 3-12.
[7] K. Wu, Y. Wu, Y. Chen, H. Chen, J. Wang, M. Yang, ChemSusChem 9 (2016) 1355-1385.
[8] I.T. Horváth, H. Mehdi, V. Fábos, L. Boda, L.T. Mika, Green Chem. 10 (2008) 238-242.
[9] H. Mehdi, V. Fábos, R. Tuba, A. Bodor, L.T. Mika, I.T. Horváth, Top. Catal. 48 (2008) 49-54.
[10] D.M. Alonso, S.G. Wettstein, J.A. Dumesic, Green Chem. 15 (2013) 584-595.
[11] Z. Xue, Q. Liu, J. Wang, T. Mu, Green Chem. 20 (2018) 4391-4408.
[12] J.M. Tukacs, D. Király, A. Strádi, Gy. Novodárszki, Zs. Eke, G. Dibó, T. Kégl, L.T. Mika, Green Chem. 14 (2012) 2057-2065.
[13] F. Li, L.M. France, Z. Cai, Y. Li, S. Liu, H. Lou, J. Long, X. Li, Appl. Catal. B 214 (2017) 67-77.

[14] A.M.R. Galletti, C. Antonetti, V. De Luise, M. Martinelli, Green Chem. 14 (2012) 688-694.
[15] J.C. Serrano-Ruiz, J.A. Dumesic, Energy Environ. Sci. 4 (2011) 83–99.
[16] DM. Zhang, FY. Ye, YJ. Guan, YM. Wang, E.J.M. Hensen, RSC Adv. 4 (2014) 39558-39564.
[17] I. Obregón, I. Gandarias, A. Ocio, I. García-García, N.A. de Eulate, P.L. Arias, Appl. Catal. B 210 (2017) 328-341.
[18] J.P. Lange, R. Price, P.M. Ayoub, J. Louis, L. Petrus, L. Clarke, H. Gosselink, Angew. Chem., Int. Ed. 49 (2010) 4479- 4483.
[19] X.-L. Du, Q.-Y. Bi, Y.-M. Liu, Y. Cao, H.-Y. He, K.-N. Fan, Green Chem. 14 (2012) 935-939.
[20] M.G. Al-Shaal, A. Dzierbinski, R. Palkovits, Green Chem. 16 (2014) 1358-1364.
[21] Q. Xu, X. Li, T. Pan, C. Yu, J. Deng, Q. Guo, Y. Fu, Green Chem. 18 (2016) 1287-1294.
[22] S.C. Patankar, G.D. Yadav, ACS Sustainable Chem. Eng. 3 (2015) 2619-2630.
[23] J.Q. Bond, D. Wang, D.M. Alonso, J.A. Dumesic, J. Catal. 281 (2011) 290-299.
[24] K. Kon, W. Onodera, K. Shimizu, Catal. Sci. Technol. 4 (2014) 3227-3234.
[25] F.M.A. Geilen, B. Engendahl, A. Harwardt, W. Marquardt, J. Klankermayer, Angew. Chem., Int. Ed. 49 (2010) 5510-5514.
[26] C.E. Chan-Thaw, M. Marelli, R. Psaro, N. Ravasio, F. Zaccheria, RSC Adv. 3 (2013) 1302-1306.
[27] J.A. Dumesic, J.C.S. Ruiz, R.M. West, US Pat. 0149922, 2012.
[28] G. Dayma, F. Halter, F. Foucher, C. Togbe, C. Mounaim-Rousselle, P. Dagaut, Energy Fuels 26 (2012) 4735–4748.
[29] Gy. Novodárszki, J. Valyon, Á. Illés, S. Dóbé, M.R. Mihályi, React. Kinet., Mech. Catal. 121(1) (2017) 275-292.
[30] E.P. Parry, J. Catal. 2 (1963) 371-379.
[31] Y. Zhao, N.E. Schultz, D.G. Truhlar, J. Chem: Theory Comput. 2 (2006) 364-382.
[32] R.A. Kendall, T.H. Dunning Jr., R.J. Harrison, J. Chem. Phys. 96 (1992) 6796-6806.
[33] M.J. Frisch, G.W. Trucks, H.B. Schlegel, G.E. Scuseria, M.A. Robb, J.R. Cheeseman, J.A. Montgomery, Jr., T. Vreven, K.N. Kudin, J.C. Burant, J.M. Millam, S.S. Iyengar, J. Tomasi, V. Barone, B. Mennucci, M. Cossi, G. Scalmani, N. Rega, G.A. Petersson, H. Nakatsuji, M. Hada, M. Ehara, K. Toyota, R. Fukuda, J. Hasegawa, M. Ishida, T. Nakajima, Y. Honda, O. Kitao, H. Nakai, M. Klene, X. Li, J.E. Knox, H.P. Hratchian, J.B. Cross, V. Bakken, C. Adamo, J. Jaramillo, R. Gomperts, R.E. Stratmann, O. Yazyev, A.J. Austin, R. Cammi, C. Pomelli, J.W. Ochterski, P.Y. Ayala, K. Morokuma, G.A. Voth, P. Salvador, J.J. Dannenberg, V.G. Zakrzewski, S. Dapprich, A.D. Daniels, M.C. Strain, O. Farkas, D.K. Malick, A.D. Rabuck, K. Raghavachari, J.B. Foresman, J.V. Ortiz, Q. Cui, A.G. Baboul, S. Clifford, J. Cioslowski, B.B. Stefanov, G. Liu, A. Liashenko, P. Piskorz, I. Komaromi, R.L. Martin, D.J. Fox, T. Keith, M.A. Al-Laham, C.Y. Peng, A. Nanayakkara, M. Challacombe, P.M.W. Gill, B. Johnson, W. Chen, M.W. Wong, C. Gonzalez, and J.A. Pople, GAUSSIAN 03 (Revision E.01), Gaussian, Inc., Wallingford CT, 2004.
[34] J.C. Serrano-Ruiz, Dong Wang, J.A. Dumesic, Green Chem. 12 (2010) 574-577.
[35] N. Scotti, M. Dangate, A. Gervasini, C. Evangelisti, N. Ravasio, F. Zaccheria, ACS Catal. 4 (2014) 2818-2826.
[36] G.A.H. Mekhmer, H.M.M. Abd-Allah, S.A.A. Mansour, Colloids Surf. A 160 (1999) 251-259.

[37] M.R. Mihályi, Gy. Novodárszki, J. Valyon, Proceedings of the 8th International Conference on Sustainable Energy & Environmental Protection, Paisley, Scotland, 2015. pp 1-10.
[38] S. Sun, N. Tsubaki, K. Fujimoto, Appl. Catal. A 202 (2000) 121-131.
[39] Á. Szegedi, M. Popova, V. Mavrodinova, Ch. Minchev, Appl. Catal. A 338 (2008) 44-51.
[40] Á. Szegedi, M. Popova, Ch. Minchev, J. Mater. Sci. 44 (2009) 6710-6716.
[41] G.B. Superti, E.C. Oliveira, H.O. Pastore, A. Bordo, C. Bisio, L. Marchese, Chem. Mater. 19 (2007) 4300-4315.
[42] G. Pál-Borbély, A. Auroux, Stud. Surf. Sci. Catal. 94 (1995) 55-62.
[43] W. Schwieger, K. Pohl, U. Brenn, C.A. Fyfe, H. Grondey, G. Fu, G.T. Kokotailo, Stud. Surf. Sci. Catal. 94 (1995) 47-55.
[44] A. Zecchina, S. Bordiga, G. Spoto, D. Scarano, G. Spano, F. Geobaldo, J. Chem Soc., Faraday Trans. 92(23) (1996) 4863-4875.
[45] S. Coluccia, L. Marchese, G. Martra, Microporous Mesoporous Mater. 30 (1999) 43-56.
[46] J.M. Eyster, E.W. Prohofsky, Spectrochim. Acta 30A (1974) 2041-2046.
[47] P. Larkin, in "Infrared and Raman Spectroscopy; Principles and Spectral Interpretation", Elsevier Inc., 2011, Ch. 8.
[48] A.P. Kilimov, M.A. Svechnilova, V.I. Shevchenko, V.V. Smirnov, F.V. Kvasnyuk-Mudryl, S.B. Zotov, Chem. Heterocycl. Compd. 3(4) (1967) 579-584.
[49] D.P. McDermott, J. Phys. Chem. 90 (1986) 2569-2574.
[50] B. Cadioli, E. Gallinella, C Coulombeau, H. Jobic, G. Berthier, J. Phys. Chem. 97 (1993) 7844-7856.
[51] C.A. Tulk, D.D. Klug, J.A. Ripmeester, J. Phys. Chem. A 102 (1998) 8734-8739.
[52] T.A. Egerton, A.H. Hardin, Y. Kozirovski, N. Sheppard, J. Catal. 32 (1974) 343-361.
[53] Nguyen The Tam, R.P. Cooney, G. Curthoys, J. Colloid Interface Sci. 51 (1975) 340-344.
[54] S.C. Ringwald, J.E. Pemberton, Environ. Sci. Technol. 34 (2000) 259-265.
[55] L. Marchese, A. Frache, E. Gianotti, G. Martra, M. Causa, S. Coluccia, Microporous Mesoporous Mater. 30 (1999) 145-153.
[56] R.M. Silverstein, F.X. Webster, D.J. Kiemle, in "Spectrometric Identification of Organic Compounds", John Wiley & Sons Inc., 7th edition, 2005, Ch. 2.
[57] L.J. Bellamy, in "The Infrared Spectra of Complex Molecules", Chapman & Hall, London, 3rd edition, 1975, Part 1, Ch. 2.
[58] S. Holly, P. Sohar, in "Infrared Spectroscopy", Műszaki Könyvkiadó, Budapest, 1968, Ch. 2 (in Hungarian).
[59] P. Pulay, G. Fogarasi, G. Pongor, J.E. Boggs, A. Vargha, J. Am. Chem. Soc. 105 (1983) 7073-7047.
[60] G.M. Hamminga, G. Mul, J.A. Moulijn, Chem. Eng. Sci. 59 (2004) 5479-5485.
[61] Yu.M. Mamatov, E.I. Klabunovskii, V.S. Kozhevnikov, Yu.I. Petrov, Chem. Heterocycl. Compd. 8 (1972) 263-265.
[62] R. Mariscal, P. Maireles-Torres, M. Ojeda, I. Sádaba, M. López Granados, Energy Environ. Sci. 9 (2016) 1144-1189.
[63] J.Q. Bond, D.M. Alonso, R.M. West, J.A. Dumesic, Langmuir 26 (2010)16291-16298.
[64] M.Lj. Mihailovič, S. Gojkovič, Z. Čvekovič, J. Chem. Soc., Perkin Trans. 1 (1972) 2460-2464.
[65] Á. Molnár, K. Felföldi, M. Bartók, Tetrahedron 37 (1981) 2149-2151.
[66] J.F. Haw, Phys. Chem. Chem. Phys. 4 (2002) 5431-5441.

[67] NIST Chemistry WebBook, http://webbook.nist.gov/cgi/cbook.cgi?ID=C96480&Units=SI&Mask=20#Ion-Energetics.

Table 1. Catalytic hydroconversion of GVL [a]

Catalyst	Reaction temp., °C	Conversion, mol %	Selectivity, mol %				
			2-MTHF [b]	1,4-PD [c]	PA [d]	Pentanols [e]	Others
Co/SiO_2	200	41.2	69.5	6.0	0	19.6	4.9 [f]
	250	99.0	52.9	0	0	27.5	19.6 [f]
Pt/H-MAG	250	43.5	0.4	0	91.7	0.3	7.6 [g]
	300	90.2	0	0	79.4	0.5	20.1 [g]

[a] Catalyst sample was reduced in situ in H_2 flow at 450 °C prior to the catalytic run. Conversion and selectivity values were determined at 30 bar total pressure and LHSV= 1 $g_{GVL} \cdot g_{cat.}^{-1} \cdot h^{-1}$. [b] 2-methyl-tetrahydrofurane. [c] 1,4-pentanediol. [d] Pentanoic acid. [e] 1-pentanol and 2-pentanol. [f] Butane, pentane, 2-pentanone, 2-butanone, 1-butanol and 2-butanol. [g] Mainly pentyl valerate and small amount of pentanal and 1-pentanol.

Table 2. Interatomic distances (in Å) in H-bonds and in GVL H-bonded to silica surface (calculated at the MP2/cc-pVDZ level).

Structure	free GVL	S1	S2	S3
C=O	1.206	1.217	1.212	1.227
Carbonyl O···H bond (1)	-	1.803	2.011	1.912
Carbonyl O···H bond (2)	-	N/A	N/A	1.956
Ring O···H bond	-	N/A	1.975	N/A
O-H bond in carbonyl O···H bond (1)	-	0.981	0.971	0.978
O-H bond in carbonyl O···H bond (2)		N/A	N/A	0.978
O-H bond in ring O···H-bond	-	N/A	0.973	N/A
O-H not involved in H-bond	-	0.964	0.966	0.967
O-H not involved in H-bond	-	0.964	0.968	0.967

Table 3. Frequency of the C=O bond stretch mode (cm^{-1}) in free GVL and in GVL adsorbed on silica surface in structures S1-S3 calculated at different levels of electronic structure theory.

Structure	free GVL	S1	S2	S3
Unscaled frequencies				
M05-2X/cc-pVDZ	1930	1879	1890	1833
M05-2X/cc-pVTZ	1898	1857	1862	1815
MP2/cc-pVDZ	1872	1834	1855	1803
MP2/cc-pVTZ	1849	1818	1831	N/A
Scaled frequencies				
M05-2X/cc-pVDZ	1782	1727	1737	1684
M05-2X/cc-pVTZ	1782	1737	1742	1698
MP2/cc-pVDZ	1782	1743	1763	1714
MP2/cc-pVTZ	1782	1751	1764	N/A

Scheme 1. Suggested reaction routes in the hydroconversion of GVL [3,9,10,18,22,23,34].

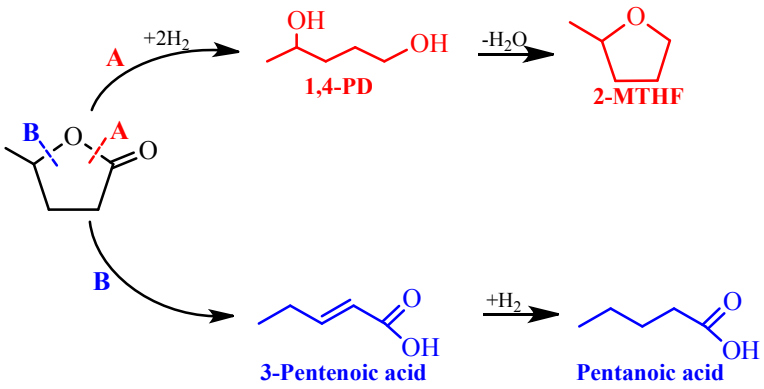

Scheme 2. Proposed reaction routes for the hydroconversion of GVL on Co/SiO_2 and Pt/H-MAG catalysts.

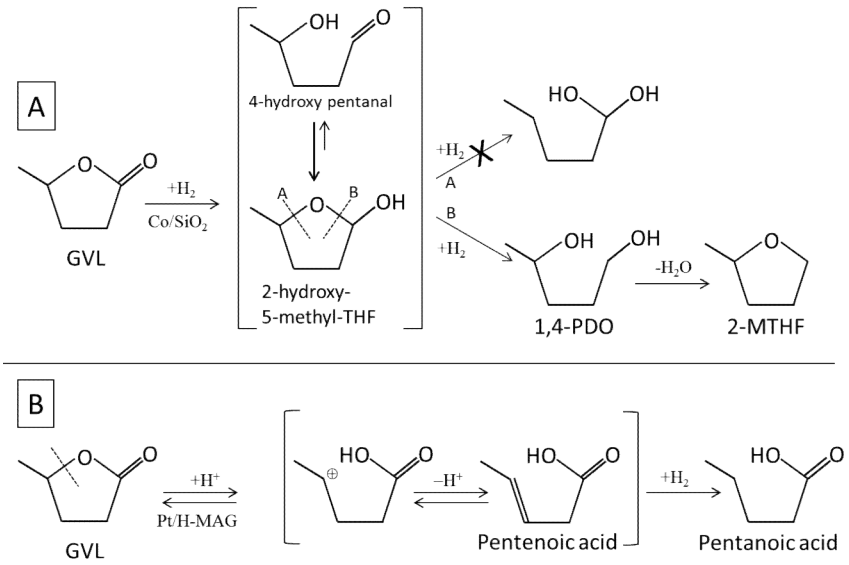

Figure Captions

Fig. 1. (A) Infrared spectra of pyridine (Py) adsorbed on *(a-c)* Co/SiO_2 and *(d-f)* Pt/H-MAG in the region of Py ring vibrations. Activated samples were contacted with Py vapor at 5 mbar and 200 °C for 30 min then degassed in high vacuum at *(a,d)* 200 °C, *(b,e)* 300 °C, and *(c,f)* 400 °C for 30 min. Each spectrum was obtained as difference of the spectra recorded after and before Py adsorption. Labels [L] and [B] indicate the characteristic band for Py bonded to Lewis- and Brønsted acid sites, respectively. (B) XRD patterns of the activated Co/SiO_2 (a) and Pt/H-MAG (b) samples. Activation of the sample before Py adsorption or XRD measurement was carried out in situ in the IR cell or XRD chamber in H_2-flow at 450 °C for 1 hour.

Fig. 2. TEM images of Co/SiO_2 and Pt/H-MAG catalyst samples.

Fig. 3. Difference DRIFT spectra of *(a)* Co/SiO_2, *(b)* SiO_2 support, and *(c)* Pt/H-MAG in contact with a continuous flow of 430 ppm GVL/H_2 mixture at 35 °C.

Fig. 4. Difference DRIFT spectra in the range of ν_{CO} stretching and C-H deformation vibrations of *(a)* Co/SiO_2, *(b)* SiO_2 support, and *(c)* Pt/H-MAG in contact with a continuous flow of 430 ppm GVL/H_2 mixture at 35 °C. Spectrum *(d)* was recorded for a thin liquid film of 10% GVL/CCl_4 solution using a liquid cell.

Fig. 5. Arrangement of atoms in typical structures of GVL adsorbed on silica. Color coding: green – C; red – O; blue – Si; white – H. Bond lengths are given in Å.

Fig. 6. IR spectra in the frequency region of carbonyl starching vibration for free GVL, and GVL adsorbed on SiO_2 support and Co/SiO_2 catalyst together with the scaled MP2/cc-pVDZ line positions calculated for the corresponding vibration for free GVL and GVL in structures S1-S3, shown in Fig. 4.

Fig. 7. (A) Difference DRIFT spectra of the species obtained from adsorption and reaction of GVL on Co/SiO_2 catalyst in the frequency range of C-H deformation vibrations. The catalyst was contacted either with a continuous flow of 430 ppm GVL/He (upper part) or with a flow of 430 ppm GVL/H_2 atmospheric gas mixture (lower part) at temperatures in the range of 35 – 225 °C (from top to bottom). Bottom spectrum (dotted line) was measured in the GVL/H_2 flow at 100 °C and 20 bar total pressure. (B) Integrated absorbance ratio of the bands at 1422 cm^{-1} ($\beta_s[CH_2(C=O)]$) and 1462 cm^{-1} ($\beta_s[CH_2]$) as function of temperature. Absorbance values for surface species obtained from GVL/He (○), and GVL/H_2 (●) gases were taken from part (A) of the figure.

Fig. 8. (A) Difference DRIFT spectra of the species obtained from adsorption and reaction of GVL on Pt/H-MAG catalyst in the frequency range of C-H deformation vibrations. The catalyst was contacted either with a continuous flow of 430 ppm GVL/He (upper part) or with a flow of 430 ppm GVL/H_2 atmospheric gas mixture (lower part) at temperatures in the range of 35 – 150 °C (from top to bottom). (B) Integrated absorbance ratio of the bands at 1355 cm^{-1} ($\delta[CH(O)]$) and 1390 cm^{-1} ($\delta_s[CH_3]$) as function of temperature. Absorbance values for surface species obtained from GVL/He (○), and GVL/H_2 (●) gases were taken from part (A) of the figure.

Fig. 9. (A) Difference DRIFT spectra of the species obtained from adsorption and reaction of GVL on Co/SiO_2 catalyst in the frequency range of carbonyl stretching vibrations. The catalyst was contacted with a continuous flow of 430 ppm GVL/He mixture at temperatures between 100 – 250 °C. Thin lines under the curves show the resolved component bands. (B) Normalized intensities (integrated absorbance) of the resolved component bands at 1760 (□), 1740 (○), and 1710 (△) cm^{-1} in the function of temperature.

Fig. 10. (A) Difference DRIFT spectra of the species obtained from adsorption and reaction of GVL on Co/SiO_2 catalyst in the frequency range of carbonyl stretching vibrations. The catalyst was contacted with a continuous flow of 430 ppm GVL/H_2 mixture at temperatures between 100 – 250 °C. Thin lines under the curves show the resolved component bands. (B) Normalized intensities (integrated absorbance) of the resolved component bands at 1760 (□), 1740 (○), and 1710 (△) cm^{-1} in the function of temperature.

Fig. 1.

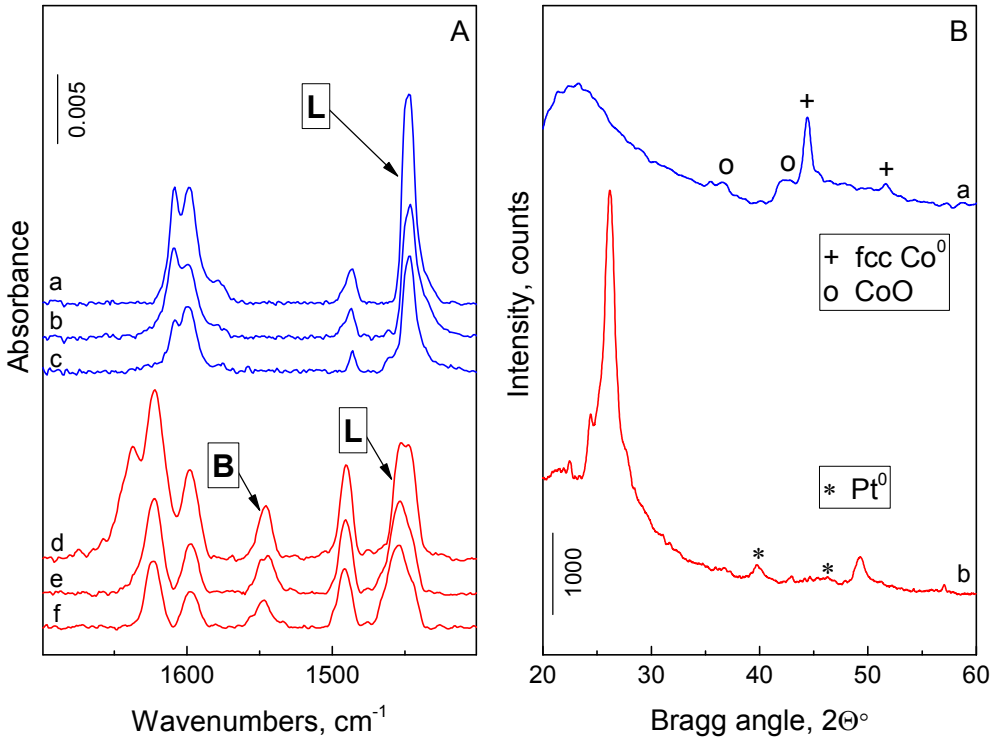
A
0.005
L
a
b
c
B
L
d
e
f
Absorbance
1600
1500
Wavenumbers, cm-1
B
+
o
o
+
a
+ fcc Co0
o CoO
* Pt0
1000
*
*
b
Intensity, counts
20
30
40
50
60
Bragg angle, 2Θ◦

Fig. 2.

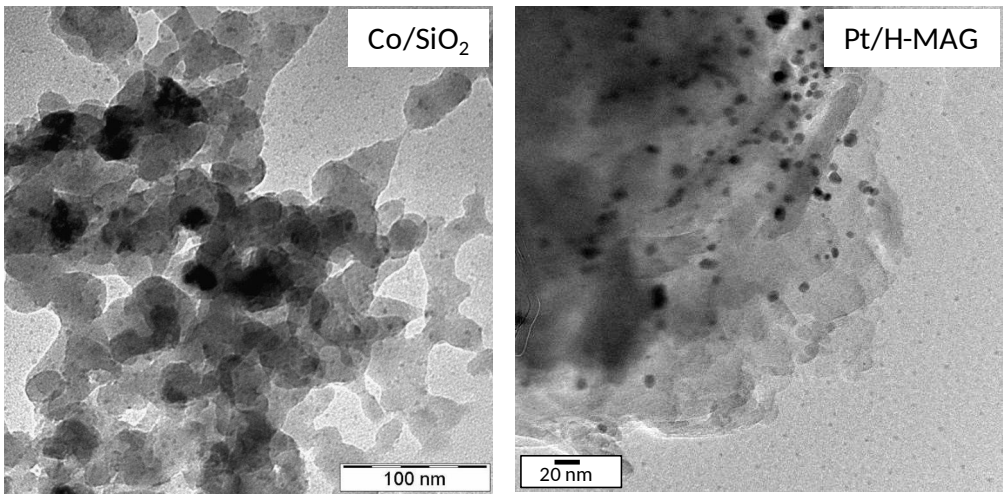

Fig. 3.

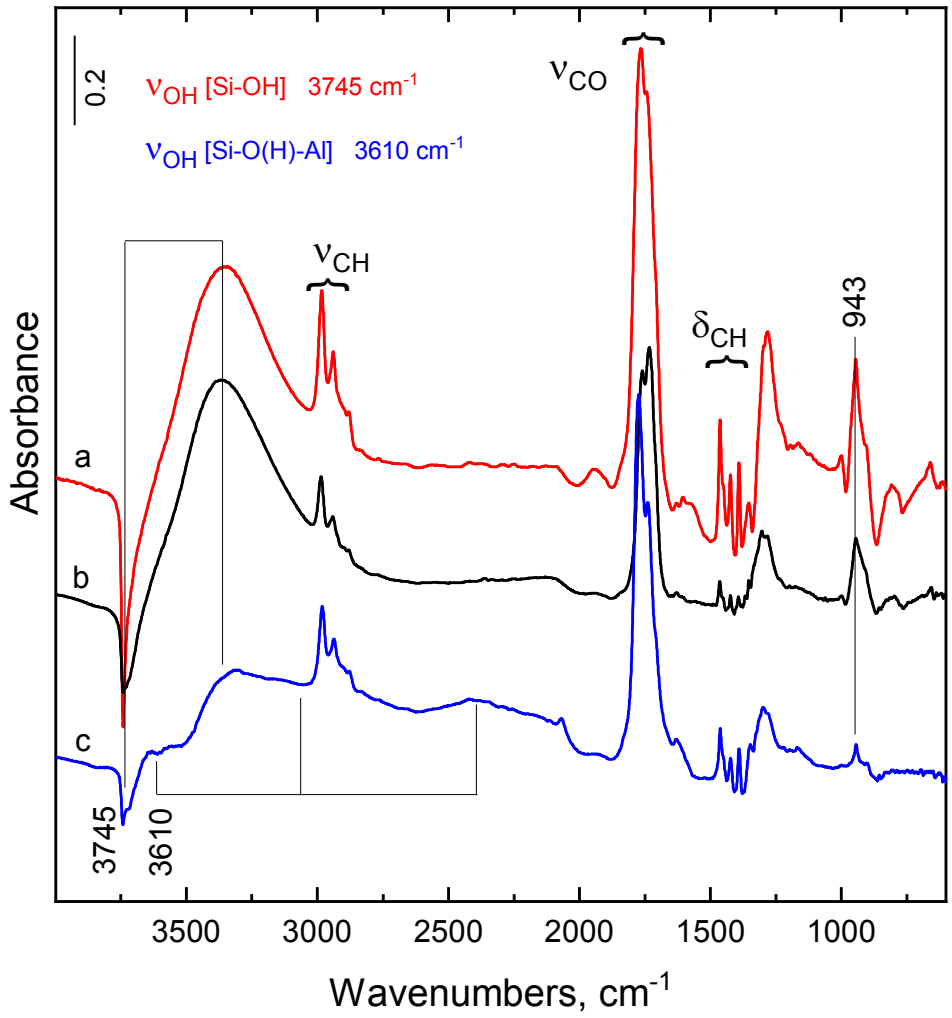
0.2
νOH [Si-OH] 3745 cm-1
νOH [Si-O(H)-Al] 3610 cm-1
νCO
νCH
δCH
943
a
b
c
3745
3610
Absorbance
3500
3000
2500
2000
1500
1000
Wavenumbers, cm-1

Fig. 4.

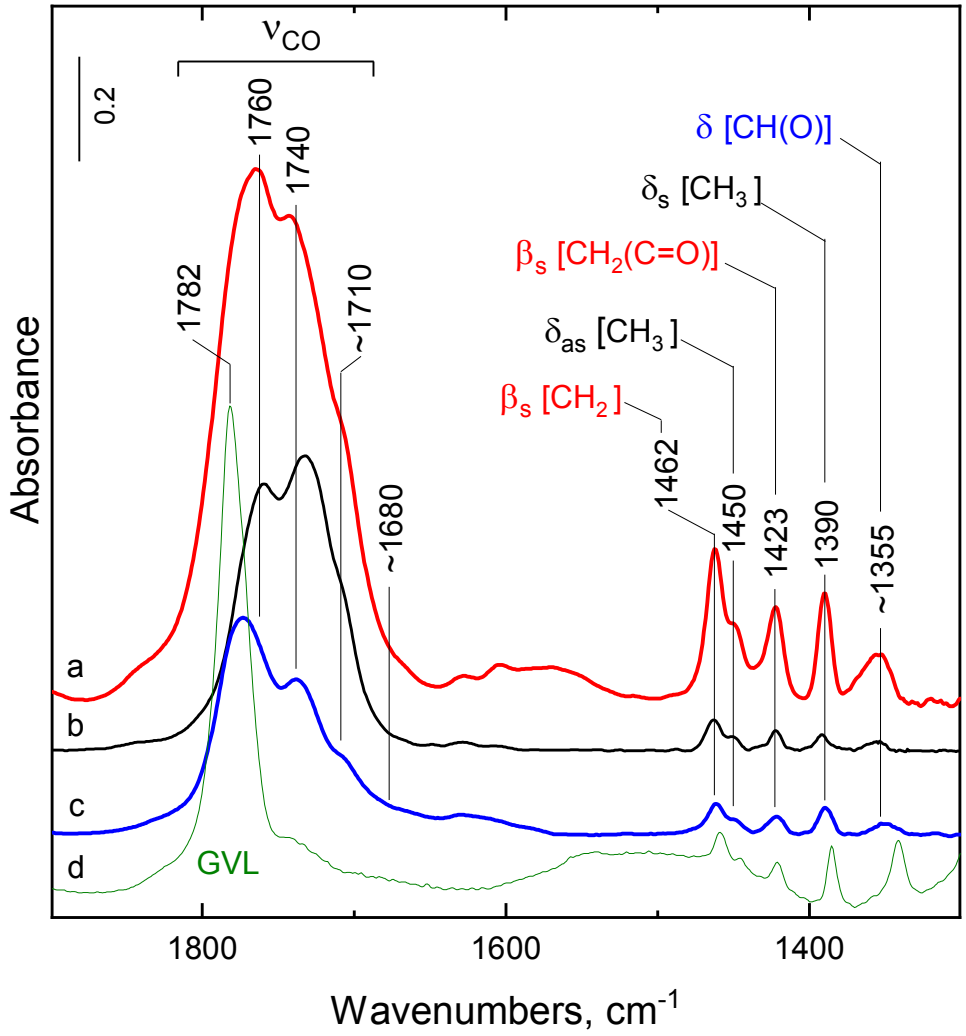
νCO
0.2
1760
1740
1782
~1710
~1680
δ [CH(O)]
δs [CH3]
βs [CH2(C=O)]
δas [CH3]
βs [CH2]
1462
1450
1423
1390
~1355
Absorbance
a
b
c
d
GVL
1800
1600
1400
Wavenumbers, cm-1

Fig. 5.

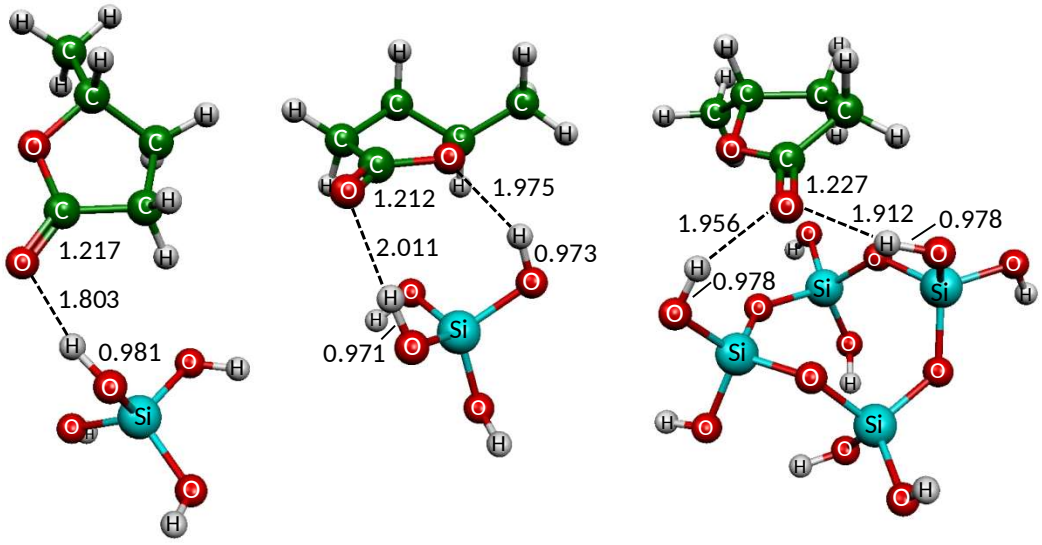
1.217
1.803
0.981
1.212
1.975
2.011
0.973
0.971
1.227
1.956
1.912
0.978
0.978
S1
S2
S3

Fig. 6.

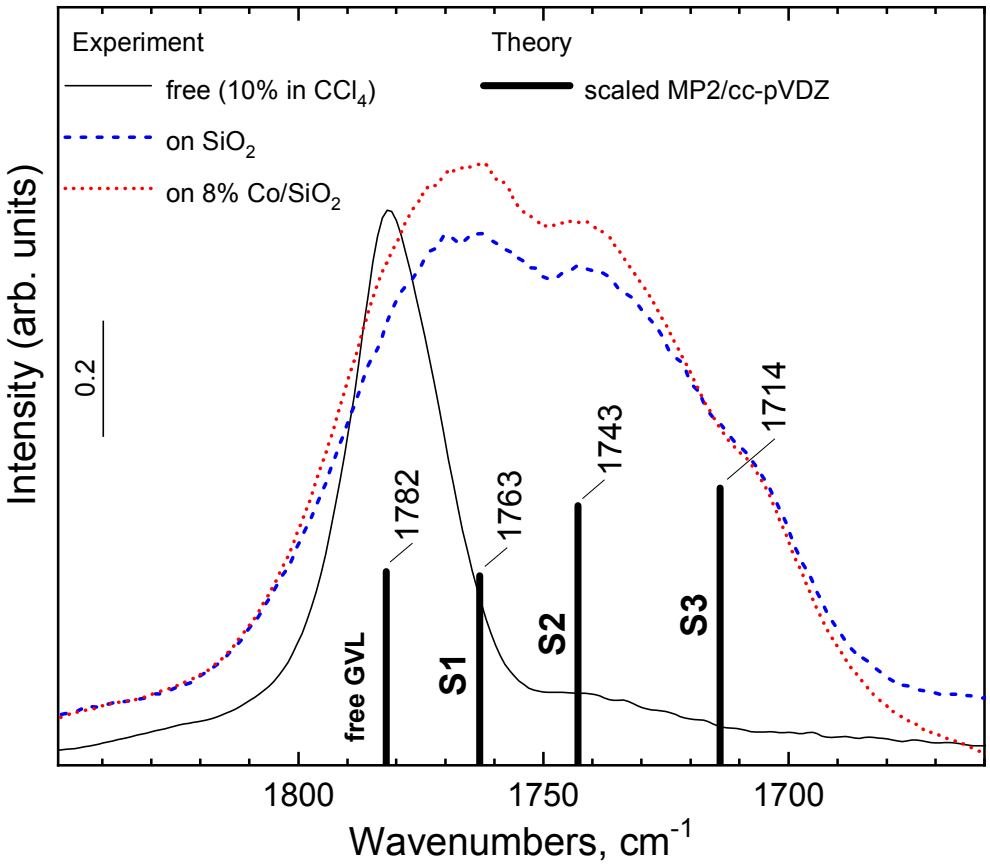
Experiment
Theory
free (10% in CCl4)
scaled MP2/cc-pVDZ
on SiO2
on 8% Co/SiO2
Intensity (arb. units)
0.2
1782
1763
1743
1714
free GVL
S1
S2
S3
1800
1750
1700
Wavenumbers, cm-1

Fig. 7.

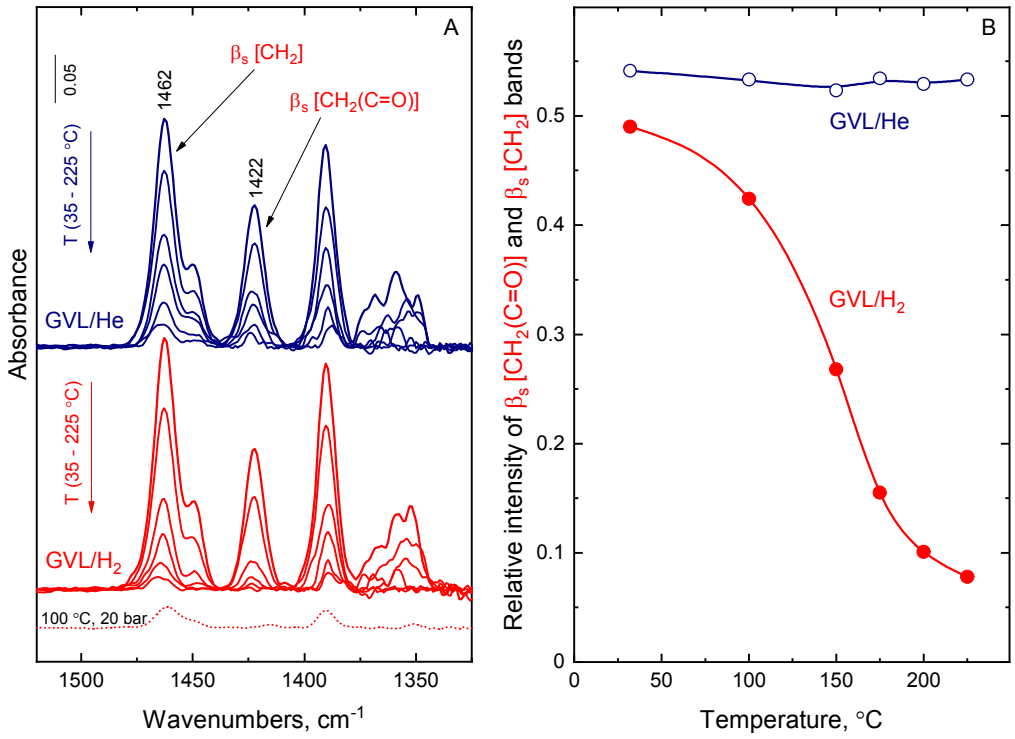
A
B
0.05
T (35 - 225 °C)
1462
1422
β_s [CH_2]
β_s [CH_2(C=O)]
GVL/He
GVL/H_2
100 °C, 20 bar
Absorbance
Wavenumbers, cm^{-1}
1500
1450
1400
1350
Relative intensity of β_s [CH_2(C=O)] and β_s [CH_2] bands
Temperature, °C
0
50
100
150
200
0.1
0.2
0.3
0.4
0.5

Fig. 8.

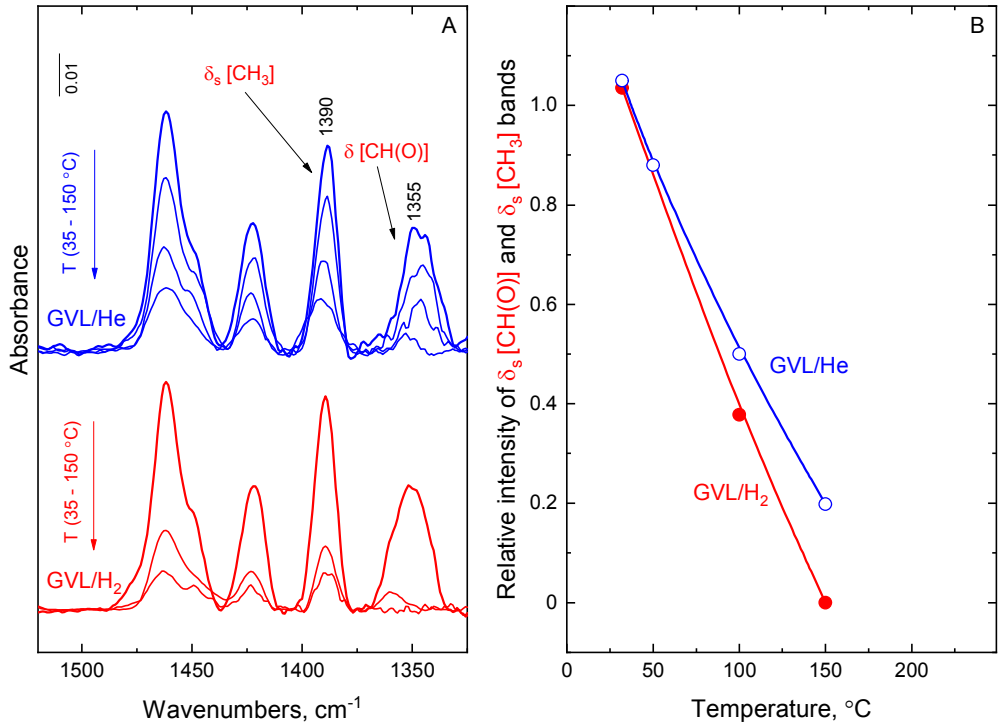
A
0.01
δs [CH3]
1390
δ [CH(O)]
1355
T (35 - 150 °C)
GVL/He
T (35 - 150 °C)
GVL/H2
Absorbance
1500
1450
1400
1350
Wavenumbers, cm-1
B
Relative intensity of δs [CH(O)] and δs [CH3] bands
1.0
0.8
0.6
0.4
0.2
0
GVL/He
GVL/H2
0
50
100
150
200
Temperature, °C

Fig. 9.

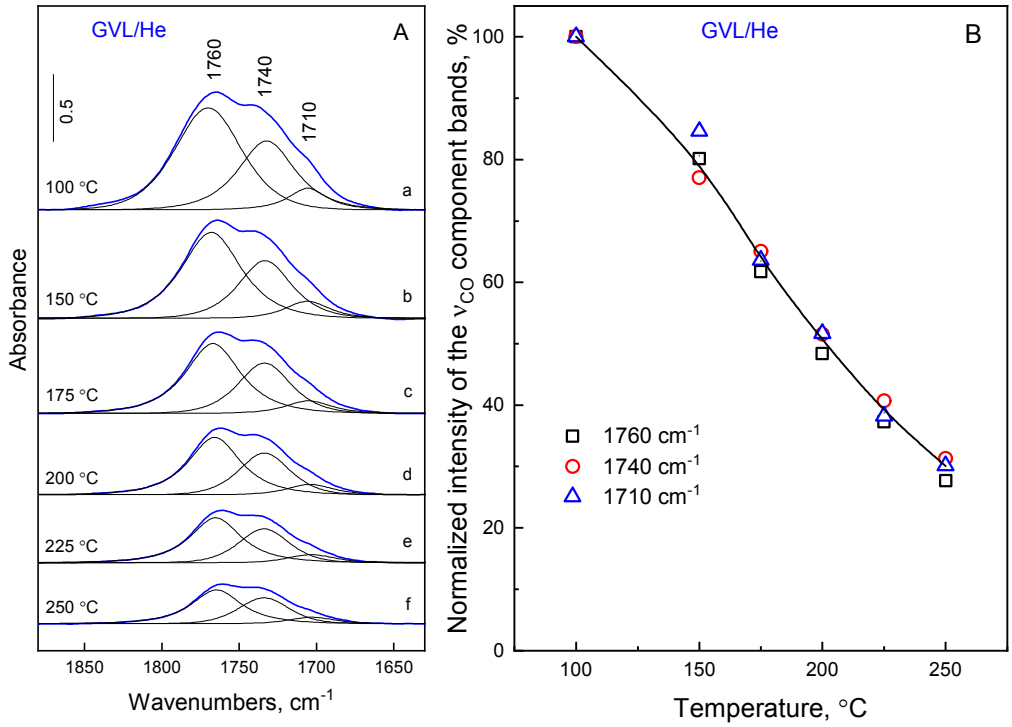
GVL/He
A
1760
1740
1710
0.5
100 °C
a
150 °C
b
175 °C
c
200 °C
d
225 °C
e
250 °C
f
Absorbance
1850
1800
1750
1700
1650
Wavenumbers, cm-1
GVL/He
B
Normalized intensity of the νCO component bands, %
100
80
60
40
20
0
1760 cm-1
1740 cm-1
1710 cm-1
100
150
200
250
Temperature, °C

Fig. 10.

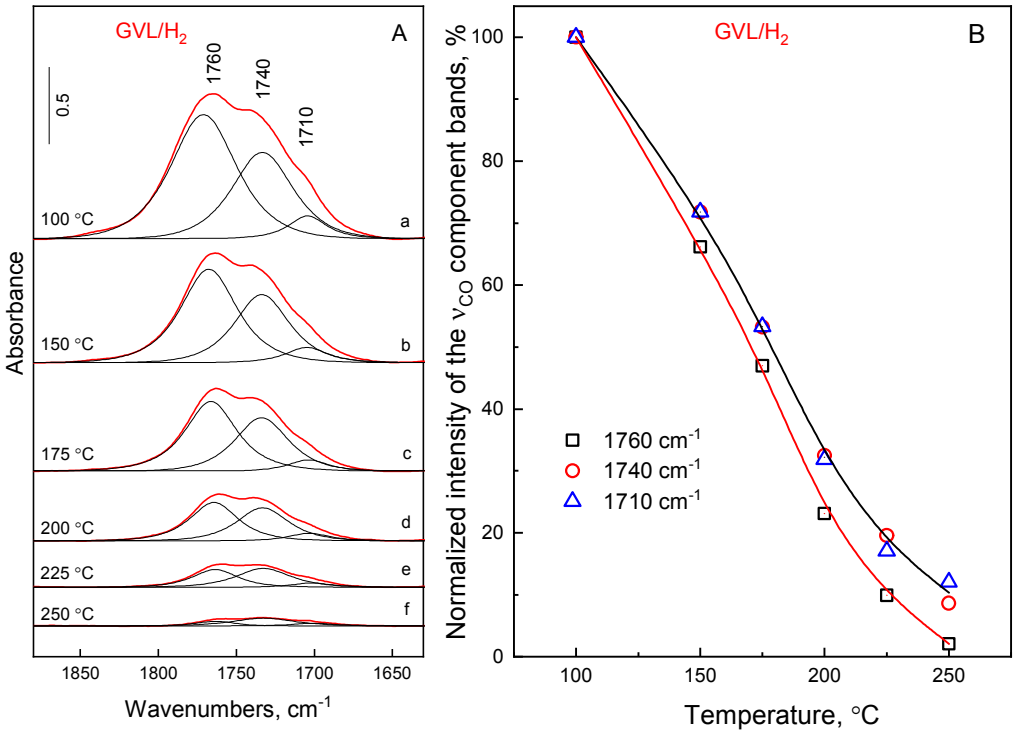
GVL/H2
A
1760
1740
1710
0.5
100 °C
a
150 °C
b
175 °C
c
200 °C
d
225 °C
e
250 °C
f
Absorbance
1850
1800
1750
1700
1650
Wavenumbers, cm-1
GVL/H2
B
Normalized intensity of the νCO component bands, %
100
80
60
40
20
0
1760 cm-1
1740 cm-1
1710 cm-1
100
150
200
250
Temperature, °C

SUPPORTING INFORMATION

Hydroconversion mechanism of biomass-derived γ-valerolactone

Gyula Novodárszki,[a] Hanna E. Solt,[a] György Lendvay,[a] R. Magdolna Mihályi,[a] Anna Vikár,[a] Ferenc Lónyi,*[a] Jenő Hancsók,[b] and József Valyon[a]

[a] *Institute of Materials and Environmental Chemistry, Research Center for Natural Sciences, Magyar tudósok körútja 2, H-1117 Budapest, Hungary. E-mail: lonyi.ferenc@ttk.mta.hu*
[b] *Department of MOL Hydrocarbon and Coal Processing, University of Pannonia, Egyetem utca 10, H-8200 Veszprém, Hungary*

Table S1. Catalytic hydroconversion of GVL [a]

Catalyst	Reaction temp., °C	Conversion, mol %	Selectivity, mol %				
			2-MTHF [b]	1,4-PD [c]	PA [d]	Pentanols [e]	Others
8%Co/SiO_2	200	41.2	69.5	6.0	0	19.6	4.9 [f]
0.5%Pt/H-MAG	250	43.5	0.4	0	91.7	0.3	7.6 [g]
4%Rh/SiO_2	250	12.1	24.0	0	60.7	11.5	3.8 [h]
0.5%Pt/Na-MAG	250	3.5	2.6	41.0	45.7	10.7	0
4%Rh-MoO_x/SiO_2	250	26.2	47.1	0.6	4.8	30.8	16.7 [i]
9%Ni/SiO_2	200	8.7	30.8	2.6	58.6	3.6	4.4 [j]
8%In,9%Ni/SiO_2	200	13.4	7.9	25.3	0	30.4	36.4 [k]

[a] Catalyst sample was reduced in situ in H_2 flow at 450 °C prior to the catalytic run. Conversion and selectivity values were determined at 30 bar total pressure and LHSV= 1 $g_{GVL} \cdot g_{cat.}^{-1} \cdot h^{-1}$. [b] 2-methyl-tetrahydrofurane. [c] 1,4-pentanediol. [d] Pentanoic acid. [e] 1-pentanol and 2-pentanol. [f] Butane, pentane, 2-pentanone, 2-butanone, 1-butanol and 2-butanol. [g] Mainly pentyl valerate and small amount of pentanal and 1-pentanol. [h] 2-butanol. [i] 2-butanol and pentanal. [j] 2-butanol. [k] pentane, 2-pentanon, 2-butanon, and 1-butanol.

The Co/SiO_2 (8%Co/SiO_2) and Pt/H-MAG (0.5%Pt/H-MAG) catalysts showed distinctively high selectivity towards 2-MTHF or PA products, respectively. The 0.5%Pt/Na-MAG catalyst (Pt supported on the non-acidic Na-form of the [Si,Al]MAG support) gave 1,4-PD, PA, and pentanols with relatively high selectivity, whereas wide variety of product selectivities was observed on the other SiO_2 supported metal catalysts.